molecular pharmaceutics

pubs.acs.org/molecularpharmaceutics

Article

Relevance of Electrostatics for the Interaction of Tyrosine Hydroxylase with Porous Silicon Nanoparticles

Maria T. Bezem,*[,§] Fredrik G. Johannessen,[§] Trond-André Kråkenes, Michael J. Sailor, and Aurora Martinez*

Cite This: *Mol. Pharmaceutics* 2021, 18, 976−985

Read Online

ACCESS | Metrics & More | Article Recommendations

ABSTRACT: Tyrosine hydroxylase (TH) is the enzyme catalyzing the rate-limiting step in the synthesis of dopamine in the brain. Developing enzyme replacement therapies using TH could therefore be beneficial to patient groups with dopamine deficiency, and the use of nanocarriers that cross the blood−brain barrier seems advantageous for this purpose. Nanocarriers may also help to maintain the structure and function of TH, which is complex and unstable. Understanding how TH may interact with a nanocarrier is therefore crucial for the investigation of such therapeutic applications. This work describes the interaction of TH with porous silicon nanoparticles (pSiNPs), chosen since they have been shown to deliver other macromolecular therapeutics successfully to the brain. Size distributions obtained by dynamic light scattering show a size increase of pSiNPs upon addition of TH and the changes observed at the surface of pSiNPs by transmission electron microscopy also indicated TH binding at pH 7. As pSiNPs are negatively charged, we also investigated the binding at pH 6, which makes TH less negatively charged than at pH 7. However, as seen by thioflavin-T fluorescence, TH aggregated at this more acidic pH. TH activity was unaffected by the binding to pSiNPs most probably because the active site stays available for catalysis, in agreement with calculations of the surface electrostatic potential pointing to the most positively charged regulatory domains in the tetramer as the interacting regions. These results reveal pSiNPs as a promising delivery device of enzymatically active TH to increase local dopamine synthesis.

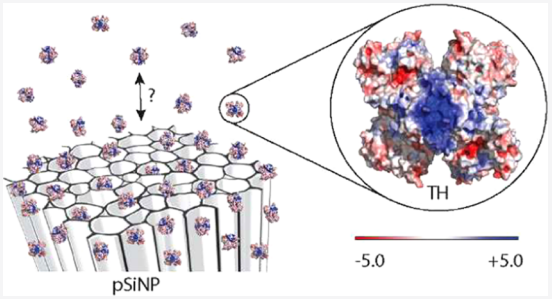

KEYWORDS: *protein aggregation, catalytic activity, enzyme replacement therapy, drug delivery, surface charge distribution*

INTRODUCTION

Tyrosine hydroxylase (TH) is a tetrameric enzyme that belongs to the family of the tetrahydrobiopterin (BH_4)-dependent aromatic amino acid hydroxylases.[1] TH catalyzes the hydroxylation of L-Tyrosine (L-Tyr) to L-3,4-dihydroxyphenylalanine (L-DOPA or levodopa), which is the rate-limiting step in the synthesis of dopamine and other catecholamine neurotransmitters.[2] Dysfunctional TH activity is associated with diseases such as TH deficiency,[3] Parkinson's disease (PD),[4] and neuropsychiatric disorders.[5,6] The traditional treatment of PD, e.g., the oral administration of levodopa, has been linked to undesirable side effects, such as dyskinesia. Other treatments include invasive surgeries like deep brain stimulation, which is often effective but includes a high risk of fatal complications of the surgery.[7] A gentler and more controlled approach to induce production of L-DOPA *in situ* in the brain is enzyme replacement therapy (ERT), for example, the delivery of TH across the blood−brain barrier (BBB) using an appropriate nanoparticle (NP) carrier.[8]

One of the main challenges for the preparation of ERT therapeutics, however, is the need to stabilize the enzyme, which is especially relevant in the case of TH, as this enzyme tends to aggregate and lose activity at 37 °C.[9] Upon interaction with phospholipid monolayers and bilayers, TH aggregates in an amyloid-like manner, causing in turn disruption of cell membranes and compromising cell viability.[10] In previous work,[11] we have shown that nanoparticles (NPs) consisting of maltodextrin with a lipid core could be used to absorb functional TH, contributing to stabilization of the enzyme and enhancing its uptake by SH-SY5Y neuroblastoma cells and brain tissue. Although these NPs cross a model of the BBB,[12] it would also be interesting to investigate interactions of TH in a more readily modifiable and biodegradable NP.

Porous silicon nanoparticles (pSiNPs) are versatile nanocarriers with several advantages; their properties are highly tunable as they are synthesized using electrochemical perforation etching where the pore size, porosity, and particle

Received: September 24, 2020
Revised: December 10, 2020
Accepted: December 28, 2020
Published: January 8, 2021

size can be controlled by the parameters of the etching procedure.[13] pSiNPs can be modified post synthesis using different surface modifications including oxidation, chemical grafting, etc.[14] These pSiNPs degrade into silicic acid, which is the biological form of silicon and an element naturally present in human tissues that has been implicated in the maintenance of bone mineral density.[15−17] Since the development of porous silicon as a biosensor in 1997,[18] the internalization of proteins into porous silicon films[19−23] or microparticles[24−26] and their various applications have been developed and investigated. Furthermore, *in vivo* biodistribution of pSiNPs, studied after intravenous injection, into mice showed some silicon content in the brain, suggesting that these pSiNPs enter the brain.[27] pSiNPs have successfully delivered siRNA to the injured brain of mice after they had been modified to improve the targeting.[28] Recently, proteins such as lysozyme[29,30] and the antibody FGK45[31] have been loaded into pSiNPs; thus, these NPs are valuable candidates as nanocarriers of proteins with the potential to be used in drug delivery. Learning more about how proteins, in general, and TH, in particular, can interact with these potential nanocarriers is therefore important.

TH is a homo-tetramer with each subunit consisting of a catalytic, regulatory, and tetramerization domain. The structure of full-length TH is not available yet, probably due to the large number of intrinsically disordered and flexible regions, but the crystal structure of the catalytic and tetramerization domains and the NMR structure of the regulatory domain are known,[32,33] which has provided a small-angle X-ray scattering (SAXS)-based full-length solution structure.[9] The isoelectric point (pI) of purified recombinant TH has been measured to be around 5.5−5.8,[34] rather similar to the theoretically calculated by the web-based software ExPASy ProtParam (pI 5.75). Thus, the net surface charge of TH is expected to be negative at neutral pH and it is therefore easily loaded onto positively charged NPs such as maltodextrin nanoparticles.[11] As pSiNPs are negatively charged, protein loading can best be achieved under or around the isoelectric point of the protein, where the protein is positively charged or neutral.[35] TH has, nevertheless, been shown to bind to negatively charged membranes at both pH 6 and 7 through its N-terminal regulatory domain, a binding that has been associated with the interaction with exposed positively charged residues.[36−38]

In this study, we investigated the interaction between the complex, unstable, and flexible TH protein with the inorganic, rigid pSiNPs, an interaction that is expected to be mainly directed by electrostatics. We investigated the effect of pH on the binding of TH to pSiNPs, as well as the effect of incorporation of TH onto NPs on the conformation, aggregation, and enzymatic activity of TH.

METHODS

Expression and Purification of Recombinant TH. Human TH, isoform TH1, was expressed and purified as described.[9] Briefly, TH was expressed in *Escherichia coli* and purified as a fusion protein with a his-tagged maltose-binding protein (MBP) using TALON Superflow Metal Affinity Resin, then cleaved with tobacco etch virus (TEV) protease, and tetrameric TH was isolated by size exclusion chromatography and stored in liquid nitrogen. Before all experiments, a TH aliquot was thawed, diluted to ca. 2 mg/mL, and centrifuged 15 min at 4 °C and 20 000*g* to remove aggregates formed during storage or freezing/thawing. The concentration of TH in the supernatant was measured using Direct Detect (Bio-Rad).

Preparation of pSiNPs. pSiNPs were prepared using electrochemical etching of silicon wafers and ultrasonic fracture, as described earlier,[13] and the resulting nanoparticles were stored in ethanol. Briefly, highly boron-doped (p++-type) silicon wafers were anodically etched in an electrolyte of 3:1 (v:v) of 48% aqueous HF:ethanol. The etching waveform consisted of alternating pulses of lower current density (50 mA/cm^2 for 1.8 s) and higher current density (400 mA/cm^2 for 0.36 s). This waveform was repeated for 140 cycles, generating a porous silicon film with alternating layers of high and low porosity. The porous silicon film was removed from the wafer by applying a low current density of 3.7 mA/cm^2 for 250 s in an electrolyte consisting of 1:10 (v:v) of 48% aqueous HF:ethanol. The freestanding porous silicon film was placed in ethanol in a sealed vial and fractured by ultrasonication (50T ultrasonic water bath, VWR International) for 12 h, and the resulting nanoparticles were collected by centrifugation (Eppendorf centrifuge model 5424R, 12 000 rpm for 10 min) and then redispersed in ethanol and stored at room temperature (RT) as a stock solution. To obtain the concentration of pSiNPs, 100 μL fractions of the stock solution were evaporated in a fume hood at RT for 24 h. The Eppendorf tubes were weighed before adding the solution, after adding the solution, and after evaporation, and the concentration was calculated from the weight difference.

Dynamic Light Scattering (DLS). The size of pSiNPs was analyzed by DLS, performed on a Zetasizer Nano ZS instrument (Malvern Panalytical), using a HeNe laser at 633 nm and a fixed scattering angle of 173° (back scatter). Measurements were performed in normal resolution mode at automatic run repetition and at room temperature in a 12 μL quartz cuvette, after a 1:10 000 dilution in either ethanol or 5 mM 4-(2-hydroxyethyl)-1-piperazineethanesulfonic acid (HEPES) pH 6.0 or 7.0, 50 mM NaCl with final concentration of 0.63 μg/mL of pSiNPs. The time-dependent stability was evaluated under the same conditions but using ZEN0040 disposable cuvettes, with 200 s intervals between preset measurements of 10 runs of 10 s each. The comparison of the interaction with TH at pH 6 and 7 was performed using 0.2 mg/mL TH and a 1:5000 dilution of pSiNPs (final concentration of 1.26 μg/mL pSiNPs) in 5 mM HEPES and 50 mM NaCl with automatic run repetition. Data analysis was performed on intensity curves and the *Z*-average size using the Malvern DTS software (Malvern Panalytical).

Thioflavin-T (ThT) Fluorescence. TH was incubated with 20 μM ThT in the presence or absence of 1:10 000 pSiNPs in 5 mM HEPES pH 6.0 or 7.0, 50 mM NaCl at RT. ThT fluorescence, with excitation at 440 nm and emission at 482 nm, was recorded in a 96-well plate every 5 min for 18 h at RT on a Synergy H1 Hybrid Reader (BioTek). Samples with only pSiNPs were used as controls and data are presented as averages of three parallel measurements. Blank measurements of buffer with corresponding pH were subtracted from the data sets.

Transmission Electron Microscopy (TEM). Sample preparation for TEM was done as following: 100 μL of a 1:1000 dilution of pSiNPs (6.3 μg/mL) alone or with 0.1 mg/mL TH and a 0.1 mg/mL TH control were incubated in an Eppendorf tube for 1 h at RT. 3 μL were carefully added onto a carbon-coated 300 mesh copper grid and left for 1 min before excess liquid was removed with tissue paper. Samples

https://dx.doi.org/10.1021/acs.molpharmaceut.0c00960
Mol. Pharmaceutics 2021, 18, 976−985

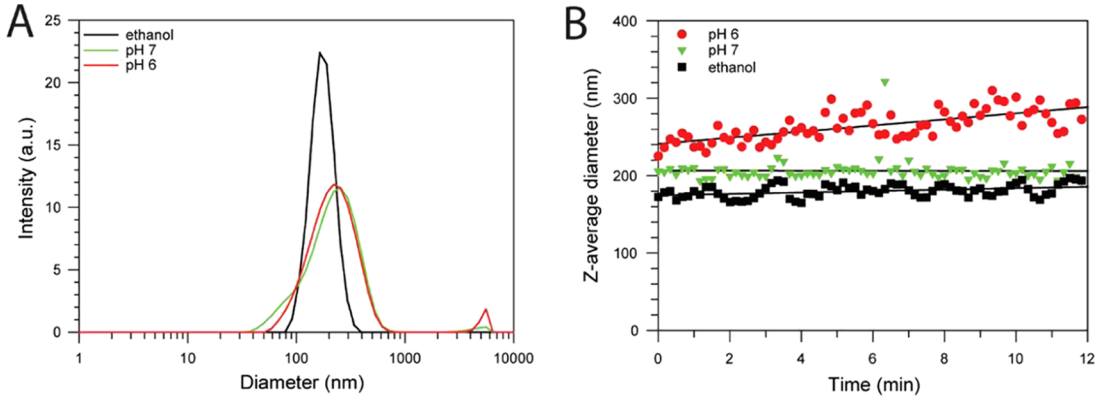

Figure 1. Size distribution and time-dependent stability of pSiNPs studied by dynamic light scattering. Representative size distribution of pSiNPs by intensity (A) at 1:10 000 dilution in ethanol (black) or 5 mM HEPES, 50 mM NaCl at pH 7 (green) or pH 6 (red) at initial dilution, at room temperature. Time-dependent stability (B) of the *Z*-average diameter of pSiNPs at 1:10 000 dilution in ethanol (black) or 5 mM HEPES, 50 mM NaCl, pH 7 (green) or pH 6 (red), with linear regression as solid black lines. Data points are the average of three independent experiments.

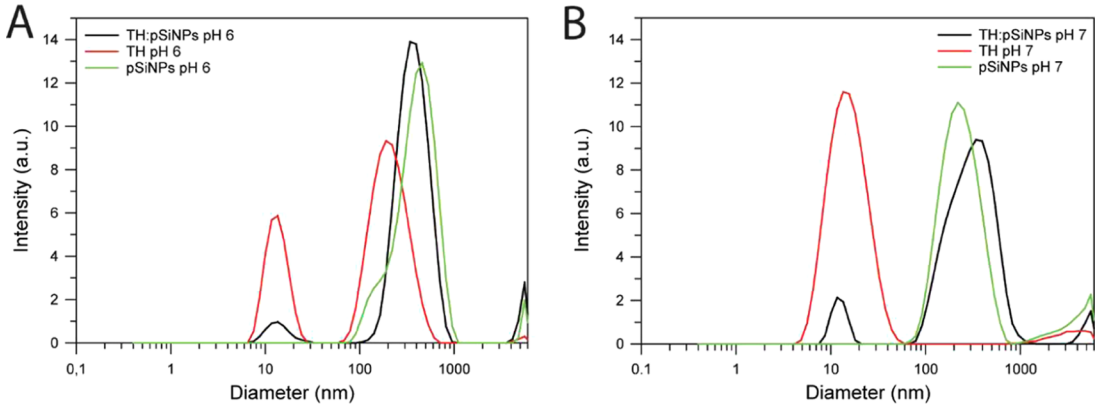

Figure 2. Size distribution of TH and its interaction with pSiNPs studied by dynamic light scattering. Intensity-based size distribution of 0.2 mg/mL TH (red), 1:5000 diluted pSiNPs (green), and both (black) at pH 6 (A) and pH 7 (B), at room temperature. The data are presented as mean of three replicates of representative loading experiments.

were negatively stained twice with 3 μL 2% uranyl acetate for 30 s each time. Images were obtained with a JEM-1230 (Jeol) TEM using 80 keV, and images were taken at 150× magnification giving 8 Å/pixel.

TH Activity. Enzymatic activity of TH was measured as described earlier,[11] with minor modifications. Briefly, TH (0.01 mg/mL) was preincubated at 37 °C with 1% bovine serum albumin (BSA) (w/v) in 5 mM HEPES pH 6.0 or 7.0, 50 mM NaCl in the absence or presence or absence of pSiNPs at 1:10 000 dilution. Aliquots of 5 μL were taken out either immediately after mixing or after 1.5 and 24 h and incubated for 1 min in a standard reaction mixture and then assayed for 5 min. The amount of L-DOPA was measured by high-performance liquid chromatography (HPLC) analysis with fluorescence detection. Controls of only pSiNPs at pH 6.0 and 7.0, and blank measurement of only buffer, showed no activity. Data are presented as an average of three parallel measurements.

Surface Electrostatic Potential Calculations. Structural analysis of TH surface electrostatics was performed at different pH values with the PDB2PQR web service,[39−41] on the SAXS-derived TH model[9] with the AMBER force field and using PROPKA to assign protonation states at different pH values. The resulting.pqr file was loaded into PyMOL (Schrödinger software, version 2.2.2) and visualized using the APBS Electrostatics plugin.

RESULTS AND DISCUSSION

Size Distribution and Stability of pSiNPs Studied by DLS. We characterized the size of pSiNPs using DLS and found that the apparent hydrodynamic diameter of pSiNPs has a peak in the size distribution at 164 nm when diluted 1:10 000 in ethanol and 220 and 255 nm in buffer at pH 6 and 7, respectively (Figure 1A). The pSiNPs were stored in ethanol after synthesis and their size remained stable at RT with a *Z*-average diameter of 180 ± 8 nm (Figure 1B). At pH 7 buffer, the *Z*-average diameter was stable at 206 ± 15 nm, whereas in pH 6 buffer, the size increased steadily from 225 ± 21 to 273 ± 20 nm over a period of 12 h (Figure 1B).

Porous silicon can be readily oxidized by OH^- present in aqueous buffers; thus, the silicon in the outer layer of pSiNP pore walls will form a SiO_2 shell which can be further oxidized into dissolvable silicic acid ($Si(OH)_4$). This process is temperature and pH dependent, with higher rates at higher pH and at higher temperatures.[14,42] pSiNPs were chosen specifically for their ability to break down in aqueous solution, and this process is expected to give an increased diameter due to the first step of the degradation where the expansion of the pore walls accommodates the extra oxygen species during the mild oxidation by OH^- in the buffer. The diameter would eventually decrease due to the second step of the degradation where silicon oxide dissolves into silicic acid. The initial

https://dx.doi.org/10.1021/acs.molpharmaceut.0c00960
Mol. Pharmaceutics 2021, 18, 976−985

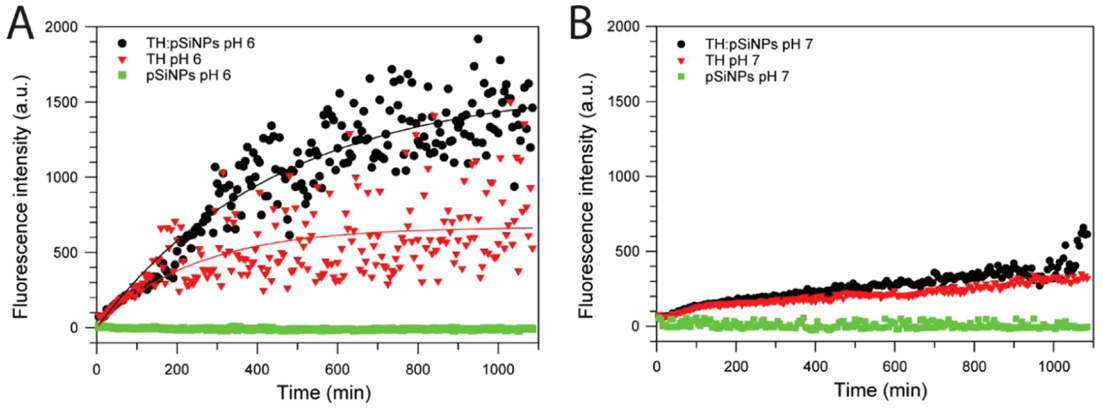

Figure 3. Aggregation propensity studied by thioflavin-T (ThT) fluorescence. Time-dependent ThT fluorescence intensity monitored at 482 nm, with excitation at 440 nm, for TH alone (red data points and line) or in the presence of pSiNPs diluted to 1:10 000 in 5 mM HEPES, 50 mM NaCl (black data points and line) at pH 6 (A) and pH 7 (B), at room temperature. Results for pure pSiNPs (no TH protein) are shown in green. The data are presented as average of three parallel measurements after subtraction of blank measurements.

difference in the diameter of pSiNPs in ethanol or the buffer solutions occurs very rapidly and cannot be captured by DLS as each measurement takes about 2 min. This difference could, however, be due to variations in the hydrodynamic shell of the solvent around pSiNPs. Another possibility is that the ions present in the buffer induce stacking or agglomeration of pSiNPs, since they have a rather flat but irregular shape.[13] This agglomeration effect increased with increasing ion concentrations, indicating that electrostatic interactions between the solvent and pSiNPs are crucial for their stability.

Size Distribution of Human TH and Its Interaction with pSiNPs. We attempted to load TH onto nanoparticles and evaluated if the enzyme could bind on the surface or within pSiNPs. Preliminary experiments showed little difference in *Z*-averages and size distributions between pH 5, 5.5, and 6 (data not shown). Since TH is known to lose its enzymatic activity gradually at pH values smaller than 7 for the human isoform 1 of TH,[43,44] we selected pH 6 as the lowest pH value to study the loading of the enzyme onto NPs. With a pI of 5.5−5.8, TH is expected to have a net negative charge at pH 7 and be almost neutral at pH 6. TH is, however, known to bind to negatively charged membranes through positively charged residues exposed on its regulatory domain. We therefore expected that the interactions between TH and pSiNPs would also happen through the regulatory domain of TH and would be more efficient at pH 6 than at pH 7 due to more favorable interactions with the negative surface charge of pSiNPs.

As measured by DLS, TH shows a size distribution with a peak around 10 nm, corresponding to the size of its tetrameric form,[9] and observed in the intensity-based size distributions at both pH 6 and pH 7 (Figure 2). TH also shows a peak corresponding to the aggregated forms of a larger diameter of 190 nm at pH 6 (Figure 2A).

We previously studied the uptake of TH onto maltodextrin NPs by DLS, following the disappearance of free tetrameric TH from solution and the concomitant increase in size of the NPs as indicated in the size distribution scans.[11] Upon addition of TH (to a final concentration of 0.2 mg/mL) to pSiNPs (with a final concentration of 1.26 μg/mL) and incubation for 1 min at RT, at either pH 6 or 7, we observed a large decrease of free TH (diameter 10−11 nm), both at pH 6 and pH 7 (Figure 2). A small increase of the pSiNP size (shift of the peak from 235 ± 54 to 322 ± 117 nm) was observed at pH 7 (Figure 2B). At pH 6, the size of pSiNPs alone partly overlapped that of aggregated TH, and DLS could thus not differentiate loaded NPs from aggregated TH (Figure 2A).

Aggregation Propensity of TH Measured by Thioflavin-T (ThT) Fluorescence. We investigated the tendency of TH to aggregate and the effect from pSiNPs on the rate of aggregate formation by monitoring the fluorescence from ThT, a dye that binds to cross-β interaction characteristic of amyloid-like aggregation.[45] It has been suggested that all proteins have a tendency to undergo this type of aggregation at certain conditions,[46] as has been previously shown for TH.[10] TH is most stable at neutral pH[43,44] and its aggregation is stimulated by interactions with lipid mono- and bilayers,[10] whereas TH aggregation is prevented by loading into maltodextrin nanoparticles.[11]

TH induces an increase in ThT fluorescence, which is more prominent at pH 6 than pH 7, and this increase is further accelerated by the presence of pSiNPs. The increase is more pronounced at pH 6 than at pH 7 (Figure 3). It seems that pSiNPs act as nucleation points for TH aggregation, which is not an unusual property of nanoparticles, as the nanoparticle surface locally increases protein concentration, promoting oligomer formation by reducing the lag phase in fibril formation.[47] Porous silicon is known to induce nucleation and is a suitable surface for protein crystallization.[48] It is also known that proteins often aggregate at the pI,[49] which can explain the higher rate of TH aggregation observed at pH 6 compared to pH 7 (Figure 3A,B).

Imaging pSiNPs, TH, and TH:pSiNP Complexes by TEM. TEM was used to investigate the interaction of TH with pSiNPs by following structural changes to the surface of pSiNPs that could be attributed to complex formation. The extensive aggregation of TH observed at pH 6, and its amplification in the presence of pSiNPs (Figure 3A) precluded the TEM study at pH 6, and we performed this study at pH 7. The pSiNPs, TH, and the mixture were diluted in 5 mM HEPES, 50 mM NaCl at pH 7.0, and incubated at RT for 1 h with final concentrations of 6.3 μg/mL pSiNPs and 0.1 mg/mL TH, before being deposited on grids, stained, and imaged. Control pSiNP samples without negative staining show irregular shapes possessing a hollow matrix with pores aligned in the same direction and spanning the whole particle diameter (Figure 4A). This is in agreement with earlier reports,[13] and the size of the nanoparticles determined by TEM is in

https://dx.doi.org/10.1021/acs.molpharmaceut.0c00960
Mol. Pharmaceutics 2021, 18, 976−985

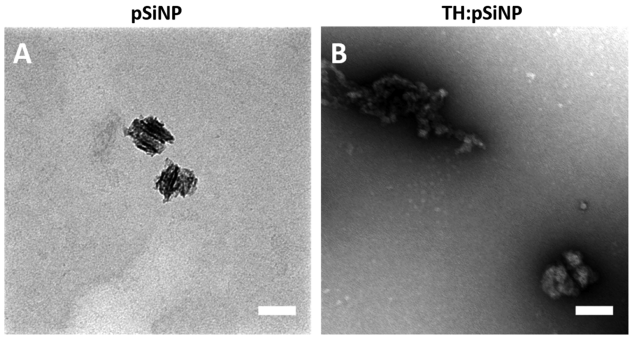

Figure 4. Transmission electron microscope (TEM) images of the interaction of TH with pSiNPs. Representative TEM images of 1:1000 pSiNPs either unstained (A) or with 0.1 mg/mL TH and negatively stained with 4% uranyl acetate (B), illustrating the interaction of TH and NPs. Both samples were prepared in 5 mM HEPES, 50 mM NaCl, pH 7. Scale bars are 100 nm.

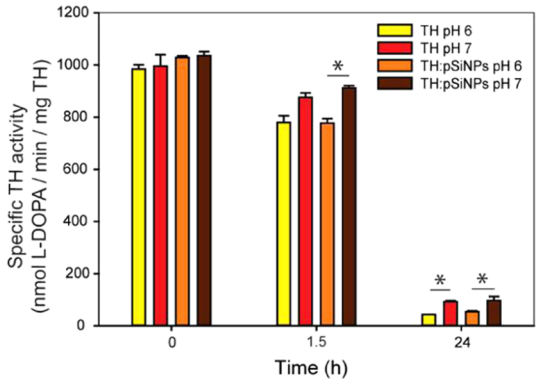

Figure 5. Effect of pSiNPs on TH activity. Specific enzymatic activity of TH *in vitro*, assayed after preincubation with and without pSiNPs at either pH 6 or 7, at 37 °C for the indicated time. Data is presented as the mean of three replicates ± standard deviation (SD). Significance was tested by a Holm−Sidak test in a one-way analysis of variance (ANOVA) and * indicates $p < 0.001$.

correspondence to the DLS results, i.e., around 150−200 nm. The pSiNPs are found as both isolated particles and clusters of particles in the TEM images.

The TH:pSiNPs mix was imaged after negative staining with 4% uranyl acetate (Figure 4B), since staining improves contrast in biological samples such as proteins. The details of the nanostructure of pSiNPs were lost in the staining, as the uranyl acetate solution stains everything but the particles, and thus only the outline of pSiNPs is visible (data not shown). The addition of TH to pSiNPs also seems to increase the incidence of NP aggregates and to smooth out the particle surface (Figure 4B), indicating that the protein resides at the particle surface. The use of TEM and negative staining facilitates the visualization of TH on NPs; however, it did not allow us to evaluate if TH was loaded into the pores of pSiNPs.

Effect of pH and pSiNPs on TH Activity. We also performed activity assays to see if the interaction with pSiNPs would have any effect on the enzymatic function of TH. The activity was assayed in a standard reaction mix at 37 °C with L-tyrosine, and the amount converted to L-DOPA by TH in the presence and absence of pSiNPs was determined by HPLC. TH activity decreased over time and was significantly lower for preincubations at pH 6 than pH 7, as earlier reported,[9,43] but pSiNPs did not seem to affect the TH activity significantly (Figure 5). This result is promising, as many enzymes lose some activity upon binding to nanoparticles, due either to partial coverage or blockage of the active site or to conformational changes.[50,51]

The relatively quick loss of TH activity has been repeatedly observed previously, both during incubation at neutral pH and temperatures in the range of 20−37 °C and under turnover, and has been found to be more pronounced for the purified enzyme than for partially purified preparations.[9,52] The loss of activity is partially associated with the reduction of conformational stability,[53] which may lead to aggregation and a nonreversible loss-of-function.[10] Moreover, it has been shown that oxidative modifications at several residues in TH inactivate the enzyme, where at least the oxidation of thiols in cysteines at controlled conditions may be reversible.[54,55] It appears that an *in vivo* environment can prevent inactivation and even regenerate inactivated TH, which is relevant for the applicability of NPs as TH nanocarriers, as shown by the increased L-DOPA production *in cellulo* after delivery of TH with maltodextrin NPs.[11] Additional TH stabilization is provided by dopamine, which is a feedback inhibitor and stabilizer of TH in brain,[9,53] and by small molecule stabilizers with pharmacological chaperone potential.[56]

Role of Electrostatics on the Binding of TH to pSiNPs. Finally, we investigated the surface electrostatics of TH in a structural model. We applied the structural model of full-length TH derived from small-angle X-ray scattering (SAXS) data as described,[9] based on known structural components, i.e., the crystal structure of the catalytic and tetramerization domains of human TH (PDB ID 2XSN; residues 157−497) and the NMR structure of the regulatory rat ACT-domain (PDB ID 2MDA; residues 71−156). *Ab initio* and homology modeling complemented with molecular dynamics simulations were used to prepare the model of the flexible N-terminal tail up to A70, and all domains and regions were combined through a SAXS-based rigid body modeling.[9] The protonation states of each residue in the model were assigned and the resulting surface electrostatic potential was visualized (Figure 6A), to provide insights on enzyme regions that may likely interact with the oxide surface of pSiNPs, which is negatively charged above pH 2.[57]

Actually, in agreement with the pI of TH, which is just below pH 6, the overall surface electrostatic potential of the enzyme is mainly negative at pH 7, whereas there are about equal amounts of negative (red) and positive (blue) patches on the surface of TH at pH 6 (Figure 6). At both pH values, the ACT-regulatory domain, corresponding to residues 71−156 in TH1, is strongly positively charged at the surface oriented away from the other domains (Figure 6A). The ACT domain thus appears particularly well suited for binding to negatively charged pSiNPs (Figures 6B and 7). A similar binding mode has also been shown for the interaction of TH to negatively charged membranes,[10] allowing the active site to be available for catalysis also in the bound state.

The regulatory ACT-domain of TH presents $\beta\beta\alpha\beta\beta\alpha$ topology,[58] where the antiparallel β-sheet is formed by the four β-strands, and the two α-helices are located, in an antiparallel orientation to each other, on the outer face of this sheet (Figure 6A and inset A, Figure 7).[33] In the dimeric ACT arrangement, the outer area presents many positively charged lysine and arginine residues, some of them are protruding from the outer surface, i.e., R89, K92, R98, K101, R137, and R138, which contribute to the positively charged surface and to the

https://dx.doi.org/10.1021/acs.molpharmaceut.0c00960
Mol. Pharmaceutics 2021, 18, 976−985

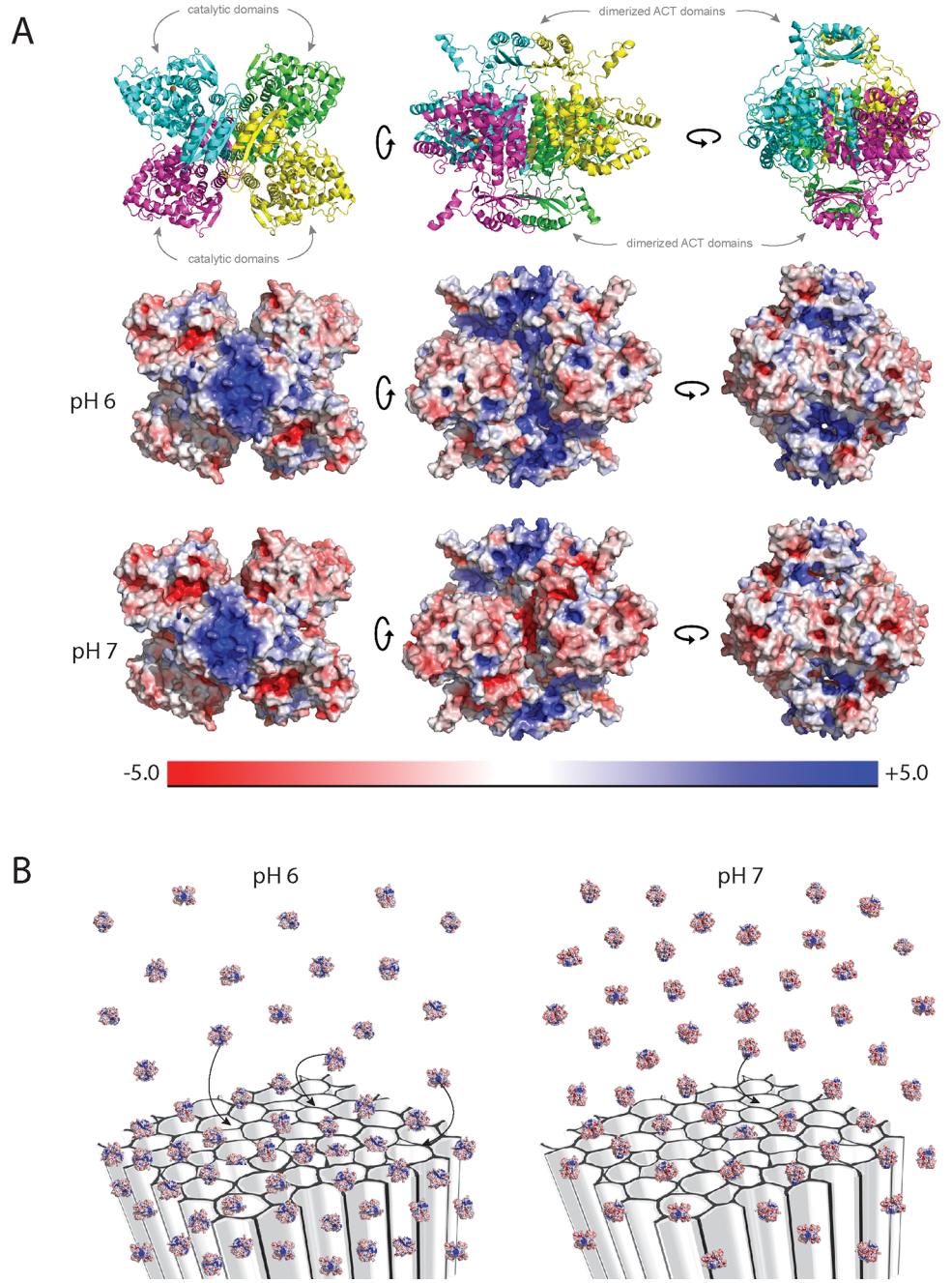

Figure 6. Effect of pH on the surface electrostatic potential of TH and its binding to pSiNPs. The modeled structure of TH and its surface electrostatic potential at pH 6 and 7 (A). At the top row, the structural model of full-length tetrameric TH prepared according to Bezem et al.[9] is shown in ribbon representation (colored by monomer and with iron atom in orange), whereas the two rows below show the surface electrostatic potential at pH 6 and 7, seen from all three orientations. Red and blue indicate negatively and positively charged regions, respectively. Illustration of pH-dependent interactions with pSiNP surfaces (B). At pH 6, which is the closest to the pI of TH, TH binds more extensively to the pSiNP surface than at pH 7. At both pH values, the ACT-regulatory domains of TH (residues 71−156) have a positively charged outer surface (blue patch) that is the most probable region binding to the pSiNP surface, as indicated by the arrows. This orients the mostly negatively charged catalytic domains away from the surface, favoring an interaction where the TH activity is retained even when bound to the nanoparticle surface.

interaction with the negatively charged pSiNP surface (see insets A, B, Figure 7). In this binding mode, the active site in the more negatively charged catalytic domain would be oriented away from the interacting region, as shown in the close-ups (Insets C, D, Figure 7), and would thus be available for catalysis. Some previous studies have shown that pH affects the orientation of the protein bound to silica nanoparticles. For instance, the model protein cytochrome c binds head-on at low pH but side-on at higher pH.[59]

Protein adsorption is not only affected by the protein properties and the pH of the solution but also influenced by factors such as temperature, the ionic strength of the solution, and the adsorbent surface properties including curvature,[60] heterogeneity, hydrophobicity,[61,62] wettability, and charge.[63] Proteins are macro zwitterions, and the distribution of charges determines the direction of their net electric dipole. Charged adsorbent surfaces exert a force on the dipole and can thereby promote a certain orientation, resulting in highly ordered

https://dx.doi.org/10.1021/acs.molpharmaceut.0c00960
Mol. Pharmaceutics 2021, 18, 976−985

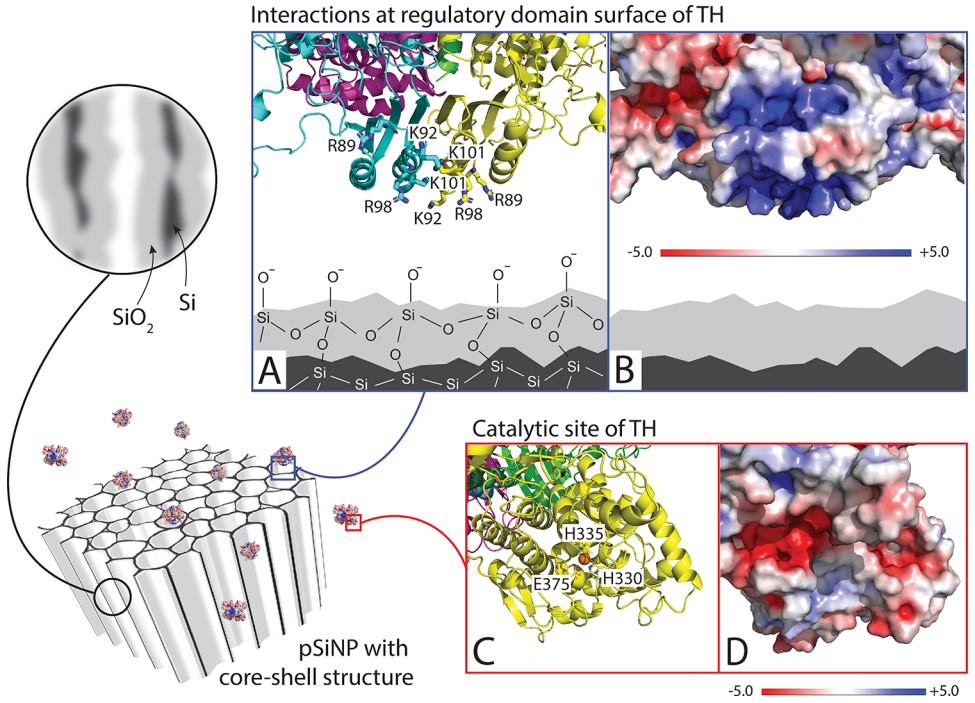

Figure 7. Possible model for the interaction of TH and pSiNPs. pSiNPs have pores of irregular shape that are aligned parallel to each other. The pore walls have a core−shell structure with a layer of silicon oxide (SiO_2) on top of pure silicon (Si), as shown in the close-up (circled in black). The oxide layer is negatively charged, onto which TH can adsorb through the positively charged patch on the outer surface of its dimeric regulatory domains, as shown in the close-ups (insets A, B). The labeled positively charged residues in the outer face of the ACT-domains are the most likely interacting residues with the pSiNP surface, and those most likely involved in the interaction are shown as sticks (inset A), whereas the surface charge distribution is shown as an electrostatic heat map of the close-up (inset B). The TH active site in the catalytic domain is oriented away from the proposed interacting region (insets C, D). The three residues coordinating the catalytic iron (orange) are shown as sticks in inset C.

layers of adsorbed protein on charged surfaces.[64] It has also been shown that it is possible to control the orientation of an adsorbing peptide through varying the electric field, either by pH or an externally applied potential.[65] The surface charge density determines the strength of the electrostatic attraction, and for enzyme haloalkane dehalogenase, the catalytic activity was preserved best upon adsorption on intermediate charged surfaces.[63] These examples show that electrostatic interactions dominate and determine the binding orientation when proteins are adsorbed onto charged surfaces and thus should be tuned for keeping the protein functional.

With respect to the penetration of TH into nanoparticle pores, we might expect that the net negative charge of TH leads to a general repulsion from the negatively charged pSiNPs and that the positively charged regulatory domains only compensate for this as long as the catalytic domains are not brought too close to pSiNPs. In the structure of tetrameric TH, the dimeric regulatory ACT-domains are located at each side and relatively far away from the butterfly-formed tetramer of catalytic domains (Figure 6A), as they are interconnected by flexible loops.[9] This arrangement suggests that TH does not penetrate much into the pores of pSiNPs but interacts primarily at the surface, as depicted in Figure 7.

Potential of pSiNP-Bound TH for Therapeutic Applications. The results presented in this study must be regarded as an initial phase in the process toward the development of therapeutic delivery of TH. Further optimization of the formulation is required for the stabilization of TH, its attachment to pSiNPs, and delivery to the brain, and the approaches to follow would depend on the route of administration.

Existing ERTs are life-long symptom relief treatments administered by intravenous injections on a regular basis, often weekly or biweekly.[66] ERT with intravenous injection of pSiNP-bound TH would require TH stabilization throughout blood circulation and subsequent uptake in the brain through the BBB. Since the pH of blood is slightly basic under normal conditions, the uptake of TH by pSiNPs should be stabilized especially at pH $\geq$ 7. This can be done by surface modifications of the pSiNP pre- or postloading of TH, to improve loading efficiency, blood circulation time, and cellular uptake. One promising modification seems to be a coating of biopolymers, such as the carbohydrates dextran and heparin, or the extracellular matrix component hyaluronic acid.[67] These polymers easily adsorb onto silicon oxide surfaces through hydrogen bonding, and a dextran coating has been shown to improve the blood half-life of pSiNPs.[27] The effect of such types of modifications must be investigated in future work. Alternatively, functional TH can be provided as an ERT to the brain through direct delivery using hydrogel implants containing TH-loaded pSiNPs. There are several reports on the regeneration of lesions in the CNS through hydrogel implantation into rat[68] or primate[69] brain, and these approaches provide a promising possibility for drug delivery through composite material.[70] Hydrogel implants for PD are a field of extensive study with regards to cell replacement therapies, sustained delivery of dopamine, or delivery of chaperone proteins such as HSP70 (See review by Giordano et al.[71] and references therein). More recently, another protein, Activin B which is a transforming growth factor, has also been delivered to the brain of a PD mouse model using an injectable hydrogel.[72] To our knowledge, there are no reports on TH

https://dx.doi.org/10.1021/acs.molpharmaceut.0c00960
Mol. Pharmaceutics 2021, 18, 976−985

delivery to the brain using a hydrogel implantation and therefore this subject warrants further investigation.

CONCLUSIONS

The properties of the interface between a nanoparticle surface, its payload, and the solvent are important for the interactions occurring in the loading of a therapeutic protein into a nanoparticle carrier. The pH, among other characteristics of the solvent, influences surface charges and can alter this binding. A better understanding of these interactions can improve loading and ensure that the therapeutic protein remains functional. We therefore investigated the relevance of the electrostatic interactions between pSiNPs and TH, an enzyme that potentially could be used to treat dopamine deficiency. TH has a net negative charge but also a well-defined patch of a positively charged surface in its ACT-regulatory domain that is oriented outwards, facilitating the binding to negatively charged surfaces such as that of pSiNPs. The size increase observed by DLS for pSiNPs upon adding TH appears in agreement with this orientation of TH upon binding at the outer surface of pSiNPs. pSiNPs induce more rapid and more extensive aggregation of TH, especially at pH 6, which we attribute to a local increase in TH concentration at the nanoparticle surface such that TH can more effectively form clusters. TH activity is not decreased significantly by the binding to pSiNPs, so its catalytic site is still accessible to substrate, indicating that it is not buried far into the pores of pSiNPs or conformationally disrupted by the interaction. We therefore conclude that TH remains functional upon binding to the pSiNP surface, which most probably happens through the positively charged patch on the surface of its regulatory domain.

AUTHOR INFORMATION

Corresponding Authors

Maria T. Bezem − *Department of Biomedicine, University of Bergen, Bergen 5009, Norway;* orcid.org/0000-0002-2022-1981; Phone: +47 98 80 11 99; Email: Maria.Bezem@uib.no

Aurora Martinez − *Department of Biomedicine, University of Bergen, Bergen 5009, Norway;* orcid.org/0000-0003-1643-6506; Phone: +47 55 58 64 27; Email: Aurora.Martinez@uib.no

Authors

Fredrik G. Johannessen − *Department of Biomedicine, University of Bergen, Bergen 5009, Norway*

Trond-André Kråkenes − *Department of Biomedicine, University of Bergen, Bergen 5009, Norway*

Michael J. Sailor − *Department of Chemistry and Biochemistry, University of California, San Diego, La Jolla, California 92093, United States;* orcid.org/0000-0002-4809-9826

Complete contact information is available at: https://pubs.acs.org/10.1021/acs.molpharmaceut.0c00960

Author Contributions

[§]M.T.B. and F.G.J. contributed equally to this work.

Author Contributions

Conception of the work: A.M. and M.J.S; collection of data: M.T.B., F.G.J., T-A.K.; analysis of data: M.T.B., F.G.J., T-A.K.; writing of manuscript: M.T.B and A.M. with contributions from all authors. All authors have given approval to the final version of the manuscript. These authors contributed equally.

Notes

The authors declare no competing financial interest.

ACKNOWLEDGMENTS

We thank Endy Spriet from the Molecular Imaging Center at the Department of Biomedicine, University of Bergen for assistance with TEM and for providing carbon-coated copper grids. We are grateful to Marte I. Flydal for purification of TH. This work was supported by grants from the Research Council of Norway (FRIMEDBIO 261826/F20), the U.S. National Science Foundation (CBET-1603177), the K.G. Jebsen Centre for Neuropsychiatric Disorders, and the Western Norway Regional Health Authorities (project 912246) (to A.M.).

REFERENCES

(1) Skjaerven, L.; Teigen, K.; Martinez, A. Structure-Function Relationships in the Aromatic Amino Acid Hydroxylases Enzyme Family: Evolutionary Insights. In *eLS*; John Wiley & Sons, Ltd., 2014.

(2) Roberts, K. M.; Fitzpatrick, P. F. Mechanisms of tryptophan and tyrosine hydroxylase. *IUBMB Life* **2013**, *65*, 350−357.

(3) Willemsen, M. A.; Verbeek, M. M.; Kamsteeg, E. J.; de Rijk-van Andel, J. F.; Aeby, A.; Blau, N.; Burlina, A.; Donati, M. A.; Geurtz, B.; Grattan-Smith, P. J.; Haeussler, M.; Hoffmann, G. F.; Jung, H.; de Klerk, J. B.; van der Knaap, M. S.; Kok, F.; Leuzzi, V.; de Lonlay, P.; Megarbane, A.; Monaghan, H.; Renier, W. O.; Rondot, P.; Ryan, M. M.; Seeger, J.; Smeitink, J. A.; Steenbergen-Spanjers, G. C.; Wassmer, E.; Weschke, B.; Wijburg, F. A.; Wilcken, B.; Zafeiriou, D. I.; Wevers, R. A. Tyrosine hydroxylase deficiency: a treatable disorder of brain catecholamine biosynthesis. *Brain* **2010**, *133*, 1810−1822.

(4) Obeso, J. A.; Rodriguez-Oroz, M. C.; Goetz, C. G.; Marin, C.; Kordower, J. H.; Rodriguez, M.; Hirsch, E. C.; Farrer, M.; Schapira, A. H.; Halliday, G. Missing pieces in the Parkinson's disease puzzle. *Nat. Med.* **2010**, *16*, 653−661.

(5) Dunčko, R.; Kiss, A.; kultetyova, I. S.; Rusnak, M.; Jezova, D. Corticotropin-releasing hormone mRNA levels in response to chronic mild stress rise in male but not in female rats while tyrosine hydroxylase mRNA levels decrease in both sexes. *Psychoneuroendocrinology* **2001**, *21*, 77−89.

(6) Dahoun, T.; Trossbach, S. V.; Brandon, N. J.; Korth, C.; Howes, O. D. The impact of Disrupted-in-Schizophrenia 1 (DISC1) on the dopaminergic system: a systematic review. *Transl. Psychiatry* **2017**, *7*, No. e1015.

(7) Deuschl, G.; Schade-Brittinger, C.; Krack, P.; Volkmann, J.; Schäfer, H.; Bötzel, K.; Daniels, C.; Deutschländer, A.; Dillmann, U.; Eisner, W.; Gruber, D.; Hamel, W.; Herzog, J.; Hilker, R.; Klebe, S.; Kloß, M.; Koy, J.; Krause, M.; Kupsch, A.; Lorenz, D.; Lorenzl, S.; Mehdorn, H. M.; Moringlane, J. R.; Oertel, W.; Pinsker, M. O.; Reichmann, H.; Reuß, A.; Schneider, G.-H.; Schnitzler, A.; Steude, U.; Sturm, V.; Timmermann, L.; Tronnier, V.; Trottenberg, T.; Wojtecki, L.; Wolf, E.; Poewe, W.; Voges, J. A Randomized Trial of Deep-Brain Stimulation for Parkinson's Disease. *N. Engl. J. Med.* **2006**, *355*, 896−908.

(8) Tosi, G.; Duskey, J. T.; Kreuter, J. Nanoparticles as carriers for drug delivery of macromolecules across the blood-brain barrier. *Exp. Opin. Drug Delivery* **2019**, 1−10.

(9) Bezem, M. T.; Baumann, A.; Skjaerven, L.; Meyer, R.; Kursula, P.; Martinez, A.; Flydal, M. I. Stable preparations of tyrosine hydroxylase provide the solution structure of the full-length enzyme. *Sci. Rep.* **2016**, *6*, No. 30390.

(10) Baumann, A.; Jorge-Finnigan, A.; Jung-Kc, K.; Sauter, A.; Horvath, I.; Morozova-Roche, L. A.; Martinez, A. Tyrosine Hydroxylase Binding to Phospholipid Membranes Prompts Its Amyloid Aggregation and Compromises Bilayer Integrity. *Sci. Rep.* **2016**, *6*, No. 39488.

(11) Bezem, M. T.; Johannessen, F. G.; Jung-KC, K.; Gundersen, E. T.; Jorge-Finnigan, A.; Ying, M.; Betbeder, D.; Herfindal, L.; Martinez, A. Stabilization of Human Tyrosine Hydroxylase in Maltodextrin Nanoparticles for Delivery to Neuronal Cells and Tissue. *Bioconjugate Chem.* **2018**, *29*, 493−502.
(12) Jallouli, Y.; Paillard, A.; Chang, J.; Sevin, E.; Betbeder, D. Influence of surface charge and inner composition of porous nanoparticles to cross blood-brain barrier in vitro. *Int. J. Pharm.* **2007**, *344*, 103−109.
(13) Qin, Z.; Joo, J.; Gu, L.; Sailor, M. J. Size Control of Porous Silicon Nanoparticles by Electrochemical Perforation Etching. *Part. Part. Syst. Charact.* **2014**, *31*, 252−256.
(14) Canham, L. *Handbook Of Porous Silicon*; Springer, 2014.
(15) Jugdaohsingh, R.; Tucker, K. L.; Qiao, N.; Cupples, L. A.; Kiel, D. P.; Powell, J. J. Dietary silicon intake is positively associated with bone mineral density in men and premenopausal women of the Framingham Offspring cohort. *J. Bone Miner. Res.* **2004**, *19*, 297−307.
(16) Carlisle, E. M. Silicon: An Essential Element for the Chick. *Science* **1972**, *178*, 619−621.
(17) Henstock, J. R.; Canham, L. T.; Anderson, S. I. Silicon: the evolution of its use in biomaterials. *Acta Biomater.* **2015**, *11*, 17−26.
(18) Lin, V. S.-Y.; Motesharei, K.; Dancil, K.-P. S.; Sailor, M. J.; Ghadiri, M. R. A Porous Silicon-Based Optical Interferometric Biosensor. *Science* **1997**, *278*, 840−843.
(19) Orosco, M. M.; Pacholski, C.; Sailor, M. J. Real-time monitoring of enzyme activity in a mesoporous silicon double layer. *Nat. Nanotechnol.* **2009**, *4*, 255−258.
(20) Andrew, J. S.; Anglin, E. J.; Wu, E. C.; Chen, M. Y.; Cheng, L.; Freeman, W. R.; Sailor, M. J. Sustained Release of a Monoclonal Antibody from Electrochemically Prepared Mesoporous Silicon Oxide. *Adv. Funct. Mater.* **2010**, *20*, 4168−4174.
(21) Rosenberg, M.; Zilony, N.; Shefi, O.; Segal, E. Designing Porous Silicon Films as Carriers of Nerve Growth Factor. *J. Vis. Exp.* **2019**, *143*, No. e58982.
(22) Arshavsky-Graham, S.; Massad-Ivanir, N.; Paratore, F.; Scheper, T.; Bercovici, M.; Segal, E. On Chip Protein Pre-Concentration for Enhancing the Sensitivity of Porous Silicon Biosensors. *ACS Sens.* **2017**, *2*, 1767−1773.
(23) De Stefano, L.; Vitale, A.; Rea, I.; Staiano, M.; Rotiroti, L.; Labella, T.; Rendina, I.; Aurilia, V.; Rossi, M.; D'Auria, S. Enzymes and proteins from extremophiles as hyperstable probes in nanotechnology: the use of D-trehalose/D-maltose-binding protein from the hyperthermophilic archaeon Thermococcus litoralis for sugars monitoring. *Extremophiles* **2008**, *12*, 69−73.
(24) Wu, C.-C.; Hu, Y.; Miller, M.; Aroian, R. V.; Sailor, M. J. Protection and Delivery of Anthelmintic Protein Cry5B to Nematodes Using Mesoporous Silicon Particles. *ACS Nano* **2015**, *9*, 6158−6167.
(25) Wang, J.; Kumeria, T.; Bezem, M. T.; Wang, J.; Sailor, M. J. Self-Reporting Photoluminescent Porous Silicon Microparticles for Drug Delivery. *ACS Appl. Mater. Interfaces* **2018**, *10*, 3200−3209.
(26) Sahare, P.; Ayala, M.; Vazquez-Duhalt, R.; Pal, U.; Loni, A.; Canham, L. T.; Osorio, I.; Agarwal, V. Enhancement of Peroxidase Stability Against Oxidative Self-Inactivation by Co-immobilization with a Redox-Active Protein in Mesoporous Silicon and Silica Microparticles. *Nanoscale Res. Lett.* **2016**, *11*, 417.
(27) Park, J. H.; Gu, L.; von Maltzahn, G.; Ruoslahti, E.; Bhatia, S. N.; Sailor, M. J. Biodegradable luminescent porous silicon nanoparticles for in vivo applications. *Nat. Mater.* **2009**, *8*, 331−336.
(28) Kang, J.; Joo, J.; Kwon, E. J.; Skalak, M.; Hussain, S.; She, Z. G.; Ruoslahti, E.; Bhatia, S. N.; Sailor, M. J. Self-Sealing Porous Silicon-Calcium Silicate Core-Shell Nanoparticles for Targeted siRNA Delivery to the Injured Brain. *Adv. Mater.* **2016**, *28*, 7962−7969.
(29) Kim, D.; Zuidema, J. M.; Kang, J.; Pan, Y.; Wu, L.; Warther, D.; Arkles, B.; Sailor, M. J. Facile Surface Modification of Hydroxylated Silicon Nanostructures Using Heterocyclic Silanes. *J. Am. Chem. Soc.* **2016**, *138*, 15106−15109.
(30) Zuidema, J. M.; Kumeria, T.; Kim, D.; Kang, J.; Wang, J.; Hollett, G.; Zhang, X.; Roberts, D. S.; Chan, N.; Dowling, C.; Blanco-Suarez, E.; Allen, N. J.; Tuszynski, M. H.; Sailor, M. J. Oriented Nanofibrous Polymer Scaffolds Containing Protein-Loaded Porous Silicon Generated by Spray Nebulization. *Adv. Mater.* **2018**, *30*, No. e1706785.
(31) Gu, L.; Ruff, L. E.; Qin, Z.; Corr, M.; Hedrick, S. M.; Sailor, M. J. Multivalent porous silicon nanoparticles enhance the immune activation potency of agonistic CD40 antibody. *Adv Mater.* **2012**, *24*, 3981−3987.
(32) Goodwill, K. E.; Sabatier, C.; Stevens, R. C. Crystal Structure of Tyrosine Hydroxylase with Bound Cofactor Analogue and Iron at 2.3 Å Resolution: Self-Hydroxylation of Phe300 and the Pterin-Binding Site. *Biochemistry* **1998**, *37*, No. 13437.
(33) Zhang, S.; Huang, T.; Ilangovan, U.; Hinck, A. P.; Fitzpatrick, P. F. The Solution Structure of the Regulatory Domain of Tyrosine Hydroxylase. *J. Mol. Biol.* **2014**, *426*, 1483−1497.
(34) Døskeland, A. P.; Flatmark, T. Ubiquitination of soluble and membrane-bound tyrosine hydroxylase and degradation of the soluble form. *Eur. J. Biochem.* **2002**, *269*, 1561−1569.
(35) Chen, M. Y.; Sailor, M. J. Charge-gated transport of proteins in nanostructured optical films of mesoporous silica. *Anal. Chem.* **2011**, *83*, 7186−7193.
(36) Thórólfsson, M.; Døskeland, A. P.; Muga, A.; Martinez, A. The binding of tyrosine hydroxylase to negatively charged lipid bilayers involves the N-terminal region of the enzyme. *FEBS Lett.* **2002**, *519*, 221−226.
(37) Halskau, Ø.; Ying, M.; Baumann, A.; Kleppe, R.; Rodriguez-Larrea, D.; Almås, B.; Haavik, J.; Martinez, A. Three-way Interaction between 14-3-3 Proteins, the N-terminal Region of Tyrosine Hydroxylase, and Negatively Charged Membranes. *J. Biol. Chem.* **2009**, *284*, 32758−32769.
(38) Skjevik, A. A.; Mileni, M.; Baumann, A.; Halskau, O.; Teigen, K.; Stevens, R. C.; Martinez, A. The N-terminal sequence of tyrosine hydroxylase is a conformationally versatile motif that binds 14-3-3 proteins and membranes. *J. Mol. Biol.* **2014**, *426*, 150−168.
(39) Dolinsky, T. J.; Nielsen, J. E.; McCammon, J. A.; Baker, N. A. PDB2PQR: an automated pipeline for the setup of Poisson-Boltzmann electrostatics calculations. *Nucleic Acids Res* **2004**, *32*, W665−W667.
(40) Baker, N. A.; Sept, D.; Joseph, S.; Holst, M. J.; McCammon, J. A. Electrostatics of nanosystems: Application to microtubules and the ribosome. *Proc. Natl. Acad. Sci. U.S.A.* **2001**, *98*, 10037−10041.
(41) APBS. poissonboltzmann.org. http://apbs.poissonboltzmann.org/pdb2pqr (14 May, 2020).
(42) Anderson, S. H. C.; Elliott, H.; Wallis, D. J.; Canham, L. T.; Powell, J. J. Dissolution of different forms of partially porous silicon wafers under simulated physiological conditions. *Phys. Status Solidi A* **2003**, *197*, 331−335.
(43) Haavik, J.; Le Bourdelles, B.; Martinez, A.; Flatmark, T.; Mallet, J. Recombinant human tyrosine hydroxylase isozymes-Reconstitution with iron and inhibitory effect of other metal ions. *Eur. J. Biochem.* **1991**, *199*, 371−378.
(44) Nasrin, S.; Ichinose, H.; Hidaka, H.; Nagatsu, T. Recombinant Human Tyrosine Hydroxylase Types 1-4 Show Regulatory Kinetic Properties for the Natural (6R)-Tetrahydrobiopterin Cofactor. *J. Biochem.* **1994**, *116*, 393−398.
(45) Aliyan, A.; Cook, N. P.; Marti, A. A. Interrogating Amyloid Aggregates using Fluorescent Probes. *Chem. Rev.* **2019**, *119*, 11819−11856.
(46) Azakami, H.; Mukai, A.; Kato, A. Role of Amyloid Type Cross â-Structure in the Formation of Soluble Aggregate and Gel in Heat-Induced Ovalbumin. *J. Agric. Food Chem.* **2005**, *53*, 1254−1257.
(47) Linse, S.; Cabaleiro-Lago, C.; Xue, W.-F.; Lynch, I.; Lindman, S.; Thulin, E.; Radford, S. E.; Dawson, K. A. Nucleation of protein fibrillation by nanoparticles. *Proc. Natl. Acad. Sci. U.S.A.* **2007**, *104*, 8691−8696.
(48) Chayen, N. E.; Saridakis, E.; El-Bahar, R.; Nemirovsky, Y. Porous silicon: an effective nucleation-inducing material for protein crystallization. *J. Mol. Biol.* **2001**, *312*, 591−595.
(49) Görg, A.; Obermaier, C.; Boguth, G.; Harder, A.; Scheibe, B.; Wildgruber, R.; Weiss, W. The current state of two-dimensial

electrophoresis with immobilized gradients. *Electrophoresis* **2000**, *21*, 1037−1053.
(50) Cha, T.; Guo, A.; Zhu, X. Y. Enzymatic activity on a chip: the critical role of protein orientation. *Proteomics* **2005**, *5*, 416−419.
(51) Liu, F.; Wang, L.; Wang, H.; Yuan, L.; Li, J.; Brash, J. L.; Chen, H. Modulating the activity of protein conjugated to gold nanoparticles by site-directed orientation and surface density of bound protein. *ACS Appl. Mater. Interfaces* **2015**, *7*, 3717−3724.
(52) Kappock, T. J.; Caradonna, J. P. Pterin-Dependent Amino Acid Hydroxylases. *Chem. Rev.* **1996**, *96*, 2659−2756.
(53) Thny, B.; Calvo, A. C.; Scherer, T.; Svebak, R. M.; Haavik, J.; Blau, N.; Martinez, A. Tetrahydrobiopterin shows chaperone activity for tyrosine hydroxylase. *J. Neurochem.* **2008**, *106*, 672−681.
(54) Sadidi, M.; Geddes, T. J.; Kuhn, D. M. S-thiolation of tyrosine hydroxylase by reactive nitrogen species in the presence of cysteine or glutathione. *Antioxid. Redox Signaling* **2005**, *7*, 863−869.
(55) Di Giovanni, G.; Pessia, M.; Di Maio, R. Redox sensitivity of tyrosine hydroxylase activity and expression in dopaminergic dysfunction. *CNS Neurol. Disord.: Drug Targets* **2012**, *11*, 419−429.
(56) Hole, M.; Underhaug, J.; Diez, H.; Ying, M.; Røhr, Å. K.; Jorge-Finnigan, A.; Fernàndez-Castillo, N.; García-Cazorla, A.; Andersson, K. K.; Teigen, K.; Martinez, A. Discovery of compounds that protect tyrosine hydroxylase activity through different mechanisms. *Biochim. Biophys. Acta, Proteins Proteomics* **2015**, *1854*, 1078−1089.
(57) Parks, G. A. The Isoelectric Points of Solid Oxides, Solid Hydroxides, and Aqueous Hydroxo Complex Systems. *Chem. Rev.* **1965**, *65*, 177−198.
(58) Lang, E. J.; Cross, P. J.; Mittelstadt, G.; Jameson, G. B.; Parker, E. J. Allosteric ACTion: the varied ACT domains regulating enzymes of amino-acid metabolism. *Curr. Opin. Struct. Biol.* **2014**, *29*, 102−111.
(59) Meissner, J.; Wu, Y.; Jestin, J.; Shelton, W. A.; Findenegg, G. H.; Bharti, B. pH-Induced reorientation of cytochrome c on silica nanoparticles. *Soft Matter* **2019**, *15*, 350−354.
(60) Yu, G.; Zhou, J. Understanding the curvature effect of silica nanoparticles on lysozyme adsorption orientation and conformation: a mesoscopic coarse-grained simulation study. *Phys. Chem. Chem. Phys.* **2016**, *18*, 23500−23507.
(61) Hung, A.; Mwenifumbo, S.; Mager, M.; Kuna, J. J.; Stellacci, F.; Yarovsky, I.; Stevens, M. M. Ordering surfaces on the nanoscale: implications for protein adsorption. *J. Am. Chem. Soc.* **2011**, *133*, 1438−1450.
(62) Peng, C.; Liu, J.; Zhao, D.; Zhou, J. Adsorption of hydrophobin on different self-assembled monolayers: the role of the hydrophobic dipole and the electric dipole. *Langmuir* **2014**, *30*, 11401−11411.
(63) Zheng, H.; Yang, S. J.; Zheng, Y. C.; Cui, Y.; Zhang, Z.; Zhong, J. Y.; Zhou, J. Electrostatic Effect of Functional Surfaces on the Activity of Adsorbed Enzymes: Simulations and Experiments. *ACS Appl. Mater. Interfaces* **2020**, *12*, 35676−35687.
(64) Quan, X.; Liu, J.; Zhou, J. Multiscale modeling and simulations of protein adsorption: progresses and perspectives. *Curr. Opin. Colloid Interface Sci.* **2019**, *41*, 74−85.
(65) Martin, L. J.; Akhavan, B.; Bilek, M. M. M. Electric fields control the orientation of peptides irreversibly immobilized on radical-functionalized surfaces. *Nat. Commun.* **2018**, *9*, No. 357.
(66) Ries, M. Enzyme replacement therapy and beyond-in memoriam Roscoe O. Brady, M.D. (1923-2016). *J. Inherited Metab. Dis.* **2017**, *40*, 343−356.
(67) Suh, K. Y.; Yang, J. M.; Khademhosseini, A.; Berry, D.; Tran, T. N.; Park, H.; Langer, R. Characterization of chemisorbed hyaluronic acid directly immobilized on solid substrates. *J. Biomed. Mater. Res., Part B* **2005**, *72*, 292−298.
(68) Hou, S.; Xu, Q.; Tian, W.; Cui, F.; Cai, Q.; Ma, J.; Lee, I. S. The repair of brain lesion by implantation of hyaluronic acid hydrogels modified with laminin. *J. Neurosci. Methods* **2005**, *148*, 60−70.
(69) Bjugstad, K. B.; Redmond, D. E.; Lampe, K. J.; Kern, D. S.; Sladek, J. R., Jr.; Mahoney, M. J. Biocompatibility of PEG-Based Hydrogels in Primate Brain. *Cell Transplant.* **2008**, *17*, 409−415.
(70) Basso, J.; Miranda, A.; Nunes, S.; Cova, T.; Sousa, J.; Vitorino, C.; Pais, A. Hydrogel-Based Drug Delivery Nanosystems for the Treatment of Brain Tumors. *Gels* **2018**, *4*, No. 62.
(71) Giordano, C.; Albani, D.; Gloria, A.; Tunesi, M.; Batelli, S.; Russo, T.; Forloni, G.; Ambrosio, L.; Cigada, A. Multidisciplinary Perspectives for Alzheimer's and Parkinson's Diseases: Hydrogels for Protein Delivery and Cell-Based Drug Delivery as Therapeutic Strategies. *Int. J. Artif. Organs* **2009**, *32*, 836−850.
(72) Li, J.; Darabi, M.; Gu, J.; Shi, J.; Xue, J.; Huang, L.; Liu, Y.; Zhang, L.; Liu, N.; Zhong, W.; Zhang, L.; Xing, M.; Zhang, L. A drug delivery hydrogel system based on activin B for Parkinson's disease. *Biomaterials* **2016**, *102*, 72−86.

https://dx.doi.org/10.1021/acs.molpharmaceut.0c00960
Mol. Pharmaceutics 2021, 18, 976−985